Tidal bores, turbulence and mixing above deep-ocean slopes

Kraig B. Winters

Scripps Institution of Oceanography
University of California San Diego
kraig@coast.ucsd.edu

Abstract

A tidally driven, stably-stratified turbulent boundary layer over steeply sloping topography is simulated numerically using a spectral LES approach. The flow is characterized by quasi-periodic, bore-like motions, with a temporal signature remarkably similar to the high-resolution ocean mooring data of van Haren (2006). The relatively thick bottom boundary layer remains stably stratified owing to the regular cycling of unmixed ambient fluid into the turbulent boundary layer and episodic expulsion events where fluid is ejected into the stratified interior. The effective diffusivity of the flow near the boundary is estimated by means of a synthetic dye tracer experiment. The simulated diffusivity and dissipation rate are in reasonable agreement with the microstructure observations of Kunze et al. (2012) when scaled to the environmental conditions at the Monterey and Soquel Canyons and to estimates of van Haren and Gostiaux (2012) from the Great Meteor Seamount in the Canary Basin.

1 Introduction

In a recent IUGG talk, McDougall et al. (2015) pointed out that the modern view of diapycnal mixing in the deep ocean is that it is bottom-intensified and caused mainly by the internal tide interacting with bottom topography. In Ferrari et al. (2016), these same authors argue that the observed decrease of kinetic energy dissipation rates with height above the bottom, combined with the hypsometry of the ocean basins, suggests that a net downwelling in the ocean interior is overcome by net upwelling along ocean boundaries. This upwelling can only be maintained by active diapycnal mixing along sloping boundaries. Moreover, they argue that "upwelling of waters along sloped topography is a pervasive characteristic of the large-scale ocean overturning circulation with important implication for the ventilation rate of the abyssal ocean."

Here, we report on a study of the dynamics of a deep-ocean stratified, turbulent boundary layer above sloping bathymetry by means of high-resolution, three-dimensional numerical simulation. The objective is to better understand the dynamics of these boundary layers and how they interact with and influence the comparatively quiescent interior basin. We also hope to understand how to best interpret moored temperature measurements given practical sampling limitations and in light of recent challenges to the use of Thorpe scale estimates of turbulence intensity (Dillon, 1982) in these particular flows.

Observations: Near-bottom measurements above steeply sloping topography typically reveal thick, stably-stratified, turbulent boundary layers characterized by strong bores with approximately semi-diurnal frequency and high dissipation rates. Good examples can be found in van Haren et al. (2015), where potential density profiles over sloping topography from moorings in the North-East Atlantic are shown at 1 second intervals with 1/2 to 1 m vertical resolution. These data extend from about 5 to 100 m above the

bottom, spanning periods of 3 weeks to 3 months, and are analyzed within intervals of 4 days or about 8 M_2 tidal periods.

The moorings were placed at 3 locations with supercritical, critical, and subcritical[1] topographic slopes. When averaged over the deepest hundred meters and 4 days, the turbulent dissipation rate ε, estimated from Thorpe scales, varied systematically from about $10^{-7}\,\mathrm{m}^2/\mathrm{s}^3$ at 2210 m depth, to $10^{-8}\,\mathrm{m}^2/\mathrm{s}^3$ at 2530 m depth, to $10^{-9}\,\mathrm{m}^2/\mathrm{s}^3$ at 2937 m depth. These depths correspond to locations where the bottom slope is supercritical, critical, and subcritical respectively. The three sites are all greater than 1400 m below the nearest topographic crest and more than 10 km away laterally.

The estimated dissipation rate above the supercritical slope is almost 1000 times greater than background levels in the ocean interior. Because these boundary layers remain stably stratified, with buoyancy frequency $N \approx 1 - 3\,\mathrm{s}^{-1}$, this near-boundary turbulence is not merely stirring already well-mixed fluid, but rather, diapycnal mixing is sustained and fluid must be continually exchanged with the comparatively quiescent stratified ambient.

Inherent & Potential Limitations of the Observations: While free-falling microstructure profilers can be used to estimate dissipation rates directly, sampling within the passage and relaxation of fast-moving bore-like signals will remain challenging-to-impossible for profiling instruments at $O(1000)$ m depth. Temporal resolution, even to 1 Hz, is possible with moored thermistor chains. These, however, typically rely on indirect estimates of the dissipation rate from Thorpe (overturning) scales l_T under the critical assumption that l_T is closely related to the Ozmidov scale L_o, where $L_o^2 \equiv \varepsilon/N^3$. Though routinely employed, this assumption has been recently challenged (Mater et al., 2015; Scotti, 2015; Chalamalla and Sarkar, 2015), in general for energetic flows with large overturns, and in particular for turbulent boundary layers driven by internal tides.

Finally, relying solely on vertical profile data tends to promote a 1D interpretation of the observations and thus a 1D view of the underlying dynamics. As Kunze et al. (2012) note, "turbulent mixing dynamics on sloping topography are fundamentally 2D or 3D in the ocean, so they cannot be accurately described by 1D models." This argument could be taken a step further to say that, because the dynamics are fundamentally 2D or 3D, it is essential to understand the influence of horizontal advection on the vertical structure of observations obtained along profiles.

2 Numerical approach

The equations of motion for three-dimensional, rotating, stratified flow under the Boussinesq approximation are integrated in time using spectral methods in a domain containing a free-slip rigid lid and a no-slip, immersed bottom boundary as shown in Figure 1. The spatial resolution extends well into the inertial subrange. The basic geometry and forcing are uniform in the x direction (out of the page), which is taken to be periodic. The initial stratification is uniform with buoyancy frequency N, and a vertical-mode-one internal tide of amplitude U_o and frequency $\sigma = M_2$ is forced at the off-shore, deep-water boundary. This excites a shoaling internal tide that impinges upon the sloping boundary. The figure is drawn to scale using the fundamental scale $\delta = U_o/N$. The slope here and in Winters (2015) is supercritical and so the incident tide back-reflects as shown.

[1]Topographic slope criticality is defined with respect to the energy propagation angle for internal waves at M_2 frequency.

The equations are augmented with high-order or "hyper-diffusion" terms that act directly only at spatial scales near the grid resolution. Owing to the fact that all derivatives are being computed spectrally, it is easy to implement high order operators that act over a known narrow band of high wavenumbers. By verifying that dissipation and mixing rates are insensitive to O(1) changes in the ad-hoc parameters of these diffusion operators, one can directly demonstrate that enough of the inertial subrange has been captured to regard the results as well-resolved large-eddy simulations (LES). At significant expense in terms of computational resources, this interpretation has been explicitly verified in Winters (2015) and Winters (2016). Sponge regions are added near the left, right, and upper boundaries to prevent reflections from reaching the analysis section.

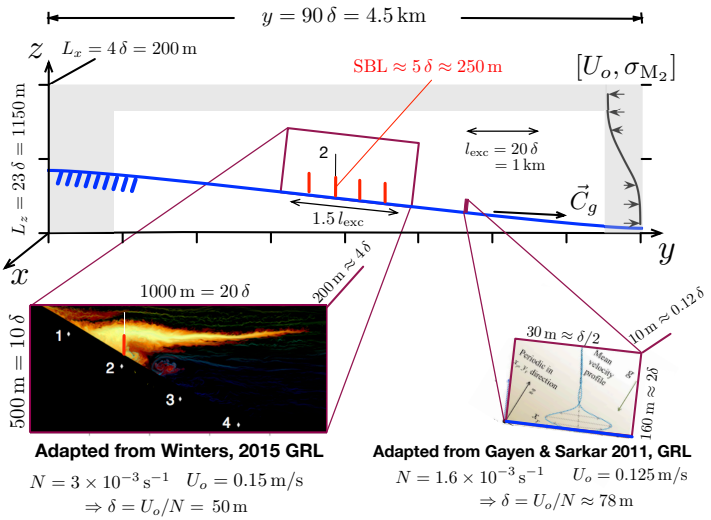

Figure 1: Schematic of the numerical simulation. A vertical-mode-one internal tide is forced offshore and propagates up-slope in a rotating, uniformly stratified fluid. Turbulent boundary layers of thickness O(5δ) (see Fig.6) develop and are indicated in red. The extent of the mooring data shown in Fig. 6 is shown in the sketch and the cut-out. Sponge regions are shaded. Horizontal and vertical lengths are shown to scale. Insets show the portion of the domain shown in Figs. 3, 4, in Winters (2015), and in Gayen and Sarkar (2011) for reference.

3 Results

Overview: The top panel of Figure 2 shows time series of temperature from fixed locations 1.7, 25, and 72 m above a supercritical, sloping bottom at about 1400 m water depth in the Bay of Biscay. The figure was adapted from van Haren (2006) who reports a characteristic vertical scale height $\delta \approx 100\,\mathrm{m}$ in an ambient stratification $N = 2.4 \times 10^{-3}\,\mathrm{s}^{-1}$. Taking $U_o = \delta\, N$ gives a characteristic speed of 0.24 m/s. Readily apparent in the near-bottom record are a series of sharp fronts, where the temperature drops suddenly as colder water advances rapidly up the slope. The fronts arrive regularly, almost but not exactly at the semi-diurnal tidal period, and are somewhat variable in their magnitude and sharpness. van Haren (2006) notes that these features are associated with up-slope, near-bottom speeds of $0.4 - 0.5\,\mathrm{m/s}$ or about $1.7 - 2.1\,U_o$. Similar features are seen in Nash et al. (2007), Martini et al. (2013) and many other near bottom records. The middle panel shows a time series constructed from density data collected above location 2 (see Figure 3) in the preliminary numerical simulation of Winters (2015). The overall character of the time series are remarkably similar, with quasi-periodic fronts of slightly variable intensity and sharpness being the distinguishing features.

The lower panel shows density as a function of height and time as the fluid sloshes back

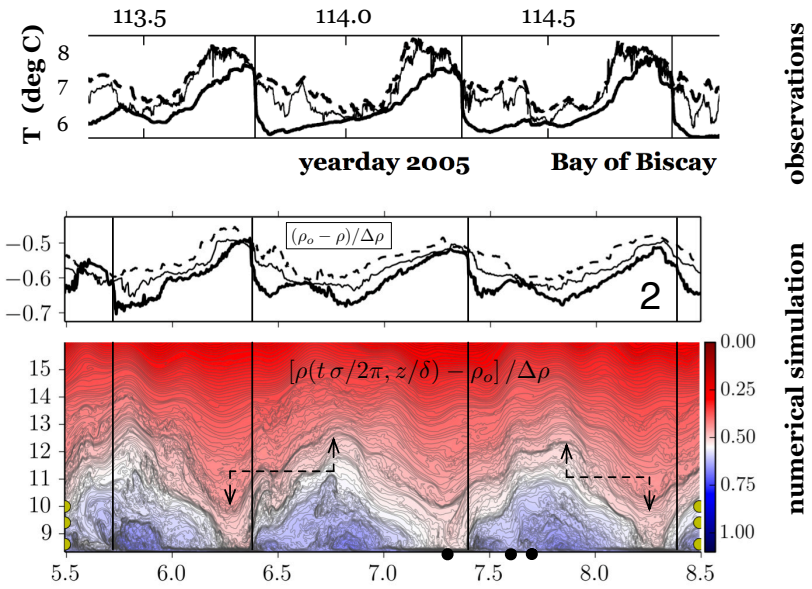

Figure 2: Lower: Density, colored and contoured as a function of height z/δ and time $t\sigma/2\pi$, from location 2 (see Figure 3, the bottom is at about $z/\delta = 8.5$.) Middle: Time series of density perturbations at heights indicated by yellow markers in lower panel. Upper: Time series of near-bottom temperature above sloping bottom in approximately 1400 m water depth in the Bay of Biscay. In all panels, vertical lines mark the arrival of bores moving upslope and the dashed lines with arrows indicate the approximate peak to peak amplitude of the isopycnal displacements. Adapted from Figure 1 of van Haren (2006), overall figure adapted from Figure 1 of Winters (2015)

and forth above location 2. In this image, the bores are the bluish patches of dense fluid that have sharp fronts and gentler tails. Within these features are trailing bores with gentler fronts. It is not clear how to objectively define a bore height or thickness, but it appears that the simulations are consistent with the observation that bore heights are greater than 50 m, or $\delta/2$, in van Haren (2006). Peak up-slope speeds associated with the bores (not shown) are about $1.5\,U_o$, consistent with the lower end of the speeds observed in the Bay of Biscay.

There are many small scale features and overturns of the isopycnals, indicative of turbulence, that extend to about $4 - 5\,\delta$ above the bottom. In addition, there are large amplitude internal wave signatures within the turbulent boundary layer itself. The dashed lines with arrows in the lower panel are visual estimates of the isopycnal displacement scale $\zeta \approx 1.25\,\delta$ within the turbulent portion of the flow. Above about 5δ from the bottom, the isopycnal surfaces vary smoothly in time and appear to be essentially wave-like.

Spatial patterns: Given the good agreement between observations obtained from ocean moorings and data extracted from the simulations on vertical profiles, we now use the numerical data to examine synoptic spatial patterns in the boundary layer flow. Detailed observations of nearly synoptic patterns can be obtained, and have proven to be useful, for tidal flows in shallow water using ship-mounted, high-frequency acoustic backscatter. Unfortunately, such patterns would be very difficult or infeasible to obtain for bottom boundary layers at depths typical of these boundary layers. Figure 3 shows snapshots of density and dye concentration in a portion of the vertical plane at $x = 0$. The upper panels, at 7.3 tidal periods, shows an up-slope propagating bore just before it reaches location 2. The head of the bore has compressed isopycnals and these compressed isopycnals curve away from the boundary and form an identifiable layer with a significantly enhanced vertical density gradient. A trailing front with denser fluid, which passes loca-

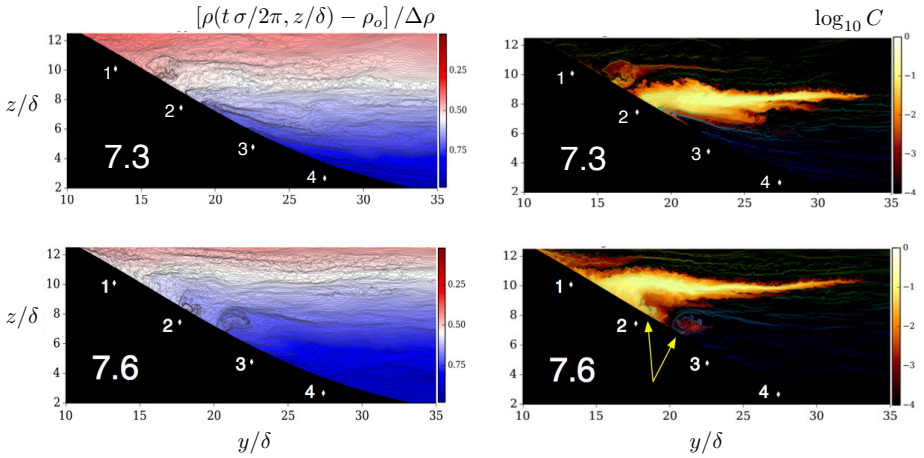

Figure 3: Snapshots of density (left) and dye concentration (right) at 7.34 and 7.64 tidal periods. Yellow arrows indicate expulsion events where near-boundary fluid is ejected into the interior. In the right panels, thin, colored isopycnals (blue to red corresponds to relatively dense to light, no colorbar shown) are superposed over the false color image. Four locations for which high-frequency time series were saved as a function of depth are indicated.

tion 2 at about 7.45 tidal periods, also compresses the isopycnals near its head and forms identifiable compressed layers that also bend away into the interior. The characteristic vertical separation between the compressed layers in the interior is about, but not exactly equal to, δ. At the same time, the flow marked by dye (upper right panel) is entraining fluid, mostly at its upper edge, which exhibits small-scale billowing patterns that extend into the interior over a lateral scale of about $15\,\delta \approx 3\,U_o/\sigma$.

By 7.6 tidal periods, flow on the upper part of the slope has reversed and begins to accelerate down-slope. Some of this relatively light fluid burrows under denser fluid near the boundary, rapidly creating a gravitationally unstable, strongly sheared flow adjacent to the slope. The flow near the boundary at greater depths has not yet reversed at this time and so a convergence zone is created that expels both density and dye near station 2 and midway between stations 2 and 3. This process also occurs further upslope at 7.3 tidal periods between stations 1 and 2, and this particular expulsion event appears to be associated with the turbulent activity on the upper flank of the dye cloud.

Diapycnal diffusivity and dissipation: The rate of near boundary mixing is estimated from the evolution of the dye concentration $C(x, y, z, t)$. Working in a domain that surrounds the dye cloud, and conditionally sampling to include only fluid parcels with $C \geq C_{min} = 10^{-4}$, the average concentration in each of many discrete density bins is computed at each time. This gives a discrete function $\overline{C}(\rho_j, t)$ for $j = 1, 2, \ldots$ where j is the bin index. The ρ_j values are then converted to nominal heights via $\bar{z}_j = (\rho_j - \rho_*)/\rho_z$, where ρ_* and ρ_z are the target density at which the dye was seeded and the ambient density gradient $-\rho_o/gN^2$ respectively. At each time, the resulting discrete distribution $\bar{C}(\bar{z}_j, t)$ is fit to a model Gaussian of the form

$$\overline{C} \approx \epsilon + C_{max}\,\exp\left\{-\left[\frac{(\bar{z}_j - z_o)^2}{2\,\sigma_{dye}^2}\right]\right\}$$

using a least squares minimization. ϵ, C_{max}, z_o and σ_{dye} are the parameters of the fit. Figure 4 shows $\overline{C}(\bar{z}_j)$ and the best fit Gaussian model at three times. For diffusion, $\sigma_{dye}^2 \sim K\,t$, where K is the effective diapycnal diffusivity of the process, and so a linear fit yields an estimate of K as the slope. The right panel shows scaled σ_{dye}^2 against scaled

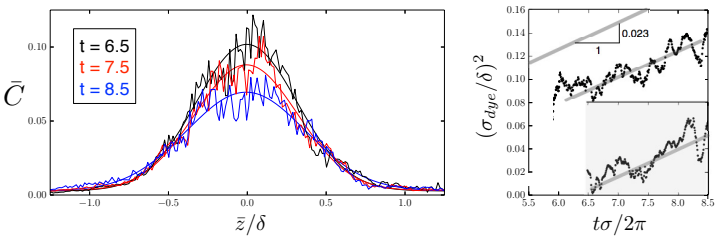

Figure 4: Left: Dye concentration $\overline{C}$ vs. height $\bar{z}/\delta$ at 6.5, 7.5 and 8.5 tidal periods. Also shown are fits to Gaussian profiles. Right: Square of the normalized width σ_{dye}/δ as a function of dimensionless time. The slope gives an estimate of the dimensionless diffusivity K, normalized by $\delta^2\,\sigma/(2\pi)$. The result of a sensitivity test in which the coefficients of the higher order operators were reduced by a factor of 2 is shown shaded and offset vertically.

time along with the best-fit slope. This value, 0.023, is thus the dimensionless diffusivity, scaled by the quantity $\delta^2/T_{\mathrm{M}_2}$. Similarly, the dissipation rate characterizing the fluid within the dye cloud itself was computed by averaging ε within the time-evolving patch defined by $C \geq C_{min}$. For the dye cloud shown in Fig. 3, the dimensionless dissipation rate, averaged over the last tidal period, is 9.7×10^{-4}, scaled by U_o^3/δ.

To scale the dimensionless results to oceanic values, one needs to specify two of the three values δ, N and U_o that characterize tidally driven boundary layers over steep slopes. To illustrate, we use the Kunze et al. (2012) observations above the sloping bottoms of Monterey and Soquel Canyons where direct dissipation rate measurements were made. There the deepest 200 m of the water column has N about $3.5 \times 10^{-3}\,\mathrm{s}^{-1}$ and isopycnal displacements ζ of $50-100$ m within the stratified, turbulent boundary layer. Taking this value of N, $\zeta = 75$ m, and using $\delta = \zeta/1.25$ (an estimate from Figure 2), gives $\delta = 60$ m, implying a velocity scale $U_o = \delta\, N = 0.21$ m/s.

With these scales, we find that the simulated flow has a diffusivity $K = 1.8 \times 10^{-3}\,\mathrm{m}^2/\mathrm{s}$ near the boundary and a tidally averaged dissipation rate $\varepsilon = 1.4 \times 10^{-7}\,\mathrm{m}^2/\mathrm{s}^3$. These values are in reasonable agreement with the corresponding values of $1.6 \times 10^{-3}\,\mathrm{m}^2/\mathrm{s}$ and $4 - 10 \times 10^{-8}\,\mathrm{m}^2/\mathrm{s}^3$ reported in Kunze et al. (2012). Similar dissipation rates, $\varepsilon = 1.5 \times 10^{-7}\,\mathrm{m}^2/\mathrm{s}^3$, were reported above a supercritical slope at the Great Meteor Seamount in the Canary Basin (van Haren and Gostiaux, 2012).

Time series and length scales: Time series of vertical velocity w at several heights within the boundary layer are shown in Fig. 5. To at least 2δ above the bottom the flow exhibits an $\omega^{-5/3}$ spectrum over about a decade and a half. This spectral slope, characteristic of homogeneous isotropic turbulence, extends from about the forcing or tidal frequency σ to frequencies significantly higher than N. There is a somewhat less extensive and less energetic $-5/3$ band at $z/\delta = 5$ but none at all by $z/\delta = 9$. Interestingly, the $-5/3$ spectral slope extends to frequencies lower than might be expected for isotropic turbulence. This signature has also been seen in turbulent boundary layers with a unidirectional mean flow, where the low frequencies can be converted to horizontal scales that are much larger than the distance to the bed or the boundary layer thickness itself (Jim Moum, personal communication). Why a demonstrably non-isotropic flow should have a $-5/3$ energy spectrum is not well understood. Longer simulations would be useful to see if this is a robust characteristic of these flows.

Length scales: Let $\rho' = \rho(z,t) - \langle\rho(z)\rangle$ where the brackets indicate temporal averaging over 3 tidal cycles and over all x, and l_b the buoyancy scale defined as $\rho'/\langle\rho_z\rangle$. Let $l_T(z,t)$ be the instantaneous Thorpe scale obtained from re-ordering each instantaneous density

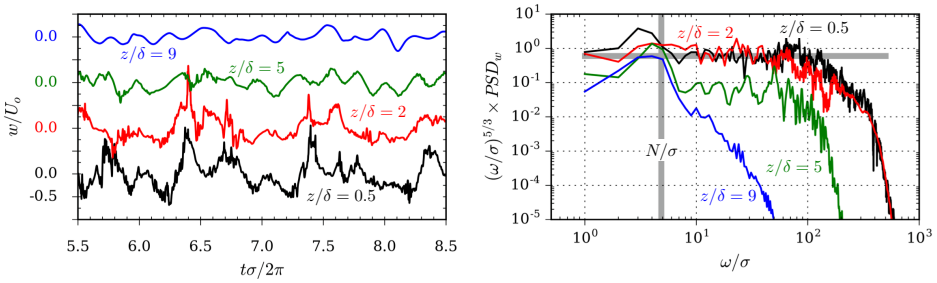

Figure 5: Left: Time series of w/U_o at 0.5, 2, 5 and 9δ above the bottom at location 2 of Fig. 3, offset vertically for clarity. Right: corresponding frequency spectra multiplied by $(\omega/\sigma)^{5/3}$ where σ is the M_2 forcing frequency.

profile. rms values were computed after averaging the squared instantaneous values in time. Here, the average is over the last tidal cycle so that a direct comparison can be made with the dissipation rate averaged over the dye-stained fluid parcels in Fig. 3. Thorpe

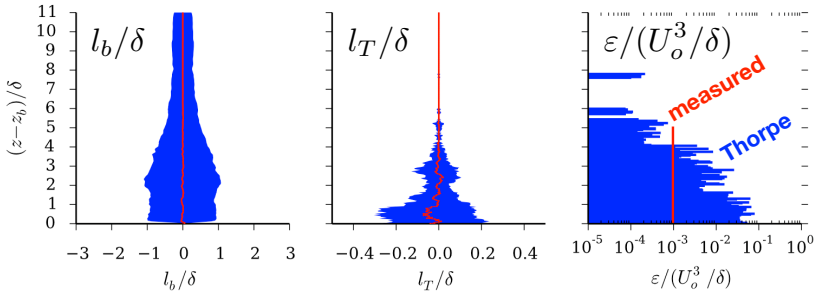

Figure 6: Mean and rms values of the buoyancy scale l_b, the Thorpe scale l_T and the dissipation rate ε as functions of height above the bottom. Also shown is the directly computed dissipation rate within the dye cloud shown in Winters (2015) which occupied a depth range of about $0 \le z/\delta < 5$. The vertical axis here is scaled height above the bottom, not absolute height as shown in Fig. 2.

scale dissipation estimates were computed as

$$\varepsilon \approx (0.8\, l_T)^2/N^3, \quad \text{assuming} \quad L_o \approx 0.8 l_T, \tag{1}$$

where at each height the instantaneous value of l_T^2 and the value of N obtained from the instantaneous sorted profile have been used. These values were then time-averaged over the last tidal cycle to produce the vertical profile shown in Fig. 6. The dissipation rate computed from Thorpe scales overestimates the true dissipation rate by about an order of magnitude: the average for $z/\delta < 5$ is 14 times the directly computed value for the dye cloud. There are, perhaps, other sampling issues to consider. The dye cloud is sloshed up and down the slope. Its average properties may not be equal to averaged properties measured at a fixed mooring position.

According to Scotti (2015), the Thorpe scale will always be larger than the Ozmidov scale in flows where relatively large overturns have both "mean" and "turbulent" components, *i.e.* in flows where not all the energy in overturns is converted to turbulence. Depending on the nature of the driving instabilities, some energy in overturns, perhaps even most, can be transferred back to non-turbulent kinetic energy. To the extent that this occurs, Eq. 1 will be an overestimate. While the theoretical argument is made contrasting shear and convectively driven turbulence, Scotti (2015) suggests in particular that $l_T >> L_o$ for wave-driven turbulence at a sloping boundary. Mater et al. (2015) and Chalamalla and Sarkar (2015) have also suggested that estimates from Thorpe scales can overestimate the dissipation rate by an order of magnitude or more. To mitigate this, Scotti (2015) advocates a filtering procedure to separate the mean from the turbulent component of l_T.

4 Conclusions

Spectral LES can be used to simulate the main features of tidally-driven stratified, deep-ocean boundary layers over sloping topography. Sufficient domain can be included to allow up-slope variability of the flow and the formation of fast-moving up-slope bores. Sufficient grid can be deployed to resolve into the inertial subrange and obtain SGS-model-independent results. Dissipation and mixing estimates are in reasonable agreement with observations. Lateral advection of turbulent fluid appears to be important in setting the vertical scale of the these boundary layers. Further study would be useful to quantify exchanges with the ambient fluid and the quantitative relationship between observable length scales.

References

Chalamalla, V. K. and Sarkar, S. (2015). Mixing, Dissipation Rate, and Their Overturn-Based Estimates in a Near-Bottom Turbulent Flow Driven by Internal Tides. *J. Phys. Oceanogr.*, 45(8):1969–1987.

Dillon, T. M. (1982). Vertical overturns: A comparison of Thorpe and Ozmidov length scales. *J. of Geophy. Res. Oceans*, 87(C12):9601–9613.

Ferrari, R., Mashayek, A., McDougall, T. J., Nikurashin, M., and Campin, J.-M. (2016). Turning ocean mixing upside down. *J. Phys. Oceanogr.*, pages DOI: 10.1175/JPO–D–15–0244.1.

Gayen, B. and Sarkar, S. (2011). Boundary mixing by density overturns in an internal tidal beam. *Geophys. Res. Lett.*, 38:L14608.

Kunze, E., MacKay, C., McPhee-Shaw, E. E., Morrice, K., Girton, J. B., and S.Terker (2012). Turbulent mixing and exchange with interior waters on sloping boundaries. *J. Phys. Oceanogr.*, 42.

Martini, K. I., Alford, M. H., Kunze, E., Kelly, S. M., and Nash, J. D. (2013). Internal bores and breaking internal tides on the oregon continental slope. *J. Phys. Oceanogr.*, 43:120–139.

Mater, B. D., Venayagamoorthy, S. K., St. Laurent, L., and Moum, J. N. (2015). Biases in Thorpe-Scale Estimates of Turbulence Dissipation. Part I: Assessments from Large-Scale Overturns in Oceanographic Data. *J. Phys. Oceanogr.*, 45(10):2497–2521.

McDougall, T., Ferrari, R., Mashayek, A., and Nikurashin, M. (2015). How does the deep ocean manage to achieve upwelling since interior diapycnal velocity is downwards? *IUGG, Ocean Mixing, Prague June 30, 2015.*

Nash, J., Alford, M., Kunze, E., Martini, K., and Kelly, S. (2007). Hotspots of deep-ocean mixing on the oregon continental slope. *Geophys. Res. Lett.*, 34.

Scotti, A. (2015). Biases in Thorpe-Scale Estimates of Turbulence Dissipation. Part II: Energetics Arguments and Turbulence Simulations. *J. Phys. Oceanogr.*, 45(10):2522–2543.

van Haren, H. (2006). Nonlinear motions at the internal tide source. *Geophys. Res. Lett.*, 33:L11605.

van Haren, H., Cimatoribus, A., and Gostiaux, L. (2015). Where large deep-ocean waves break. *Geophys. Res. Lett.*, 42:2351–2357.

van Haren, H. and Gostiaux, L. (2012). Detailed internal wave mixing above a deep-ocean slope. *J. Marine Res.*, 70:173–197.

Winters, K. B. (2015). Tidally driven mixing and dissipation in the stratified boundary layer above steep submarine topography. *Geophys. Res. Lett.*, 42(17):7123–7130.

Winters, K. B. (2016). The turbulent transition of a supercritical downslope flow: sensitivity to downstream conditions. *J. Fluid Mech.*, 792:997–1012.